

Substantial reduction of write-error rate for voltage-controlled magnetoresistive random access memory by in-plane demagnetizing field and voltage-induced negative out-of-plane anisotropy field

Rie Matsumoto, Shiniji Yuasa, Hiroshi Imamura

National Institute of Advanced Industrial Science and Technology (AIST), Tsukuba, Ibaraki 305-8568, Japan

Abstract

Voltage-controlled magnetoresistive random access memory (VC-MRAM) based on voltage-induced dynamic switching in magnetic tunnel junctions (MTJs) is a promising ultimate non-volatile memory with ultralow power consumption. However, the dynamic switching in a conventional MTJ is accompanied by a relatively high write error rate (WER), hindering the reliable operation of VC-MRAM. Here, we propose a reliable writing scheme using the in-plane demagnetizing field (IDF) and voltage-induced negative out-of-plane anisotropy field (NOAF). Numerical simulations based on macrospin model demonstrate that the voltage-induced NOAF modifies the switching dynamics and increases the torque due to the IDF, thereby reducing the switching time. The IDF and voltage-induced NOAF also reduce the mean energy difference between the magnetization direction at the end of the pulse and the equilibrium direction. As a result, an appropriate combination of the IDF and voltage-induced NOAF reduces the WER by one order of magnitude compared with that of the dynamic switching in a conventional MTJ.

Keywords: Spintronics, Voltage controlled magnetism

PACS: 75.30.Gw, 75.70.Ak, 75.78.-n, 85.75.-d

Email addresses: rie-matsumoto@aist.go.jp (Rie Matsumoto), h-imamura@aist.go.jp (Hiroshi Imamura)

1. Introduction

Voltage-controlled magnetoresistive random-access memory (VC-MRAM) [1, 2, 3, 4, 5, 6, 7, 8, 9, 10, 11, 12, 13, 14] has attracted considerable attention as an emerging ultralow-power non-volatile memory. The writing scheme of VC-MRAM is based on the voltage control of magnetic anisotropy (VCMA) in a magnetic tunnel junction (MTJ) [15, 16, 17] with perpendicular magnetization (see Fig. 1(a)). Without applied voltage, the magnetization in the FL is aligned nearly in the out-of-plane direction due to the perpendicular magnetic anisotropy (PMA) at the interface. Application of the voltage pulse (see Fig. 1(b)) reduces the PMA through the VCMA effect [1, 2, 3, 4, 5], inducing the precession of the magnetization around the magnetic field applied in the in-plane direction [18].

In the conventional dynamic switching scheme [6, 7, 8, 9, 10, 11, 12, 13, 14], the circular cylinder shaped MTJ nanopillar is used as shown Fig. 1(c). The effective out-of-plane anisotropy constant, K_{eff} , is reduced to zero by the voltage pulse, as shown in Fig. 1(d), where $K_{\text{eff}}^{(0)}$ and $K_{\text{eff}}^{(+V)}$ denote the effective out-of-plane anisotropy at $V = 0$ and $V = V_p$, respectively. The WER strongly depends on the pulse duration, t_p , as shown in Fig. 1(e). The WER is minimized when t_p is approximately the half of the precession period. The VC-MRAM has a clear advantage that its energy consumption to write a bit is one hundred times smaller than that of the spin-transfer-torque (STT)-MRAM [19, 11]. However, the WER of the VC-MRAM ($\gtrsim 10^{-6}$) [14] is considerably higher than that of the STT-MRAM ($\sim 10^{-11}$) [20]. To reduce the WER of VC-MRAM, very precise control of the pulse duration is necessary. Notably, such precise control of the pulse duration is difficult in large-scale integrated circuits due to circuit delay.

Another switching scheme of VC-MRAM called heavily damped switching [21, 22] is schematically shown in Fig. 1(f). The in-plane magnetic field is applied parallel to the minor axis of the elliptical MTJ. The Gilbert damping constant, α , is assumed to be large enough to suppress the precession back to the initial direction. The effective out-of-plane anisotropy constant is reduced by the voltage pulse but remains positive as shown in Fig. 1(g). Although the minimum WER of the heavily damped switching is higher than that of the conventional dynamic switching due to the large α , the heavily damped switching has an advantage that the WER is insensitive to the pulse duration as shown in Fig. 1(h). Therefore, the precise control of the pulse duration is unnecessary. The heavily damped switching is suited for some special

applications such as error-tolerant machine learning for image recognition and object detection [23].

For cache applications, it is necessary to develop a reliable writing scheme, whose WER is very low. In this paper, we propose a new reliable switching scheme using the in-plane demagnetizing field (IDF) and voltage-induced negative out-of-plane anisotropy field (NOAF) (Figs. 1(i) and (j)). We calculated the WER by solving the Langevin equation of the macrospin model, demonstrating that the WER is reduced by one order of magnitude (Fig. 1(k)) compared with that of the dynamic switching in a conventional MTJ (Fig. 1(e)). The mechanism of the reduction of the WER is discussed by analyzing the switching dynamics, torques, and distribution of the magnetizations at the end of the pulse.

2. Model and method

We consider an elliptical cylinder shaped MTJ nanopillar, shown in Figs. 1(a) and (i). The lateral size of the nanopillar is assumed to be so small that the magnetization dynamics can be described by the macrospin model. The direction of magnetization in the FL is represented by the unit vector $\mathbf{m} = (m_x, m_y, m_z) = (\sin \theta \cos \phi, \sin \theta \sin \phi, \cos \theta)$, where θ and ϕ are the polar and azimuthal angles, respectively. The x -axis is parallel to the major axis of the ellipse. The external in-plane magnetic field, \mathbf{H}_{ext} , is applied in the positive y -direction. The magnetization in the reference layer is fixed to align with the positive z -direction.

The energy density of the FL is given by [24]

$$\begin{aligned} \mathcal{E}(m_x, m_y, m_z) = & \frac{1}{2}\mu_0 M_s^2 (N_x m_x^2 + N_y m_y^2 + N_z m_z^2) \\ & + K_u (1 - m_z^2) - \mu_0 M_s \mathbf{m} \cdot \mathbf{H}_{\text{ext}}, \end{aligned} \quad (1)$$

where, the demagnetization coefficients N_x , N_y , and N_z are assumed to satisfy $N_z \gg N_y > N_x$, μ_0 is the vacuum permeability, M_s is the saturation magnetization of the FL, and $\mathbf{H}_{\text{ext}} = (0, H_{\text{ext}}, 0)$ is the external in-plane magnetic field. Without loss of generality, we assume that $H_{\text{ext}} > 0$. The index of the IDF, H_D is given by $H_D = M_s(N_y - N_x)$ [25]. K_u is the uniaxial out-of-plane anisotropy constant. The value of K_u can be controlled by applying a bias voltage V through the VCMA effect, as shown in Fig. 1(j). Hereafter, K_{eff} represents the effective out-of-plane anisotropy constant defined by $K_{\text{eff}} = K_u - (1/2)\mu_0 M_s^2 (N_z - N_x)$, and $K_{\text{eff}}^{(+V)}$ indicates the value

of K_{eff} during the voltage pulse. Note that, when $H_{\text{ext}} = 0$ and K_{eff} is negative (positive), the magnetization is relaxed to in-plane (perpendicular) state. We call the field induced by the negative effective out-of-plane anisotropy as negative out-of-plane anisotropy field (NOAF).

The magnetization dynamics are simulated using the following Langevin equation [26]:

$$(1 + \alpha^2) \frac{d\mathbf{m}}{dt} = -\gamma_0 \mathbf{m} \times \{(\mathbf{H}_{\text{eff}} + \mathbf{h}) + \alpha [\mathbf{m} \times (\mathbf{H}_{\text{eff}} + \mathbf{h})]\}, \quad (2)$$

where t is time, $\gamma_0 = 2.21 \times 10^5 \text{ rad} \cdot \text{s}^{-1} \cdot (\text{A}/\text{m})^{-1}$ is the gyromagnetic ratio, and α is the Gilbert damping constant. The thermal agitation field, \mathbf{h} , satisfies the following relations: $\langle h_\iota(t) \rangle = 0$ and $\langle h_\iota(t) h_\kappa(t') \rangle = [2\alpha k_B T / (\gamma_0 \mu_0 M_s \Omega)] \delta_{\iota\kappa} \delta(t - t')$, where $\langle \rangle$ represents the statistical mean, $\iota, \kappa = x, y, z$, k_B is the Boltzmann constant, T is the temperature, Ω is the volume of the FL volume, and $\delta_{\iota\kappa}$ is Kronecker's delta. The effective magnetic field, \mathbf{H}_{eff} , is defined as

$$\mathbf{H}_{\text{eff}} = -\frac{1}{\mu_0 M_s} \nabla \mathcal{E}. \quad (3)$$

The following parameters are assumed in simulations. The Gilbert damping constant is set as $\alpha = 0.1$, the saturation magnetization as $M_s = 955 \text{ kA}/\text{m}$, the effective anisotropy constant at $V = 0$ as $K_{\text{eff}}^{(0)} = 110 \text{ kJ}/\text{m}^3$, and temperature as $T = 300 \text{ K}$. Hereafter, the superscript “(0)” denotes any quantities obtained at $V = 0$. The thickness and area of the FL are $d = 1.1 \text{ nm}$ and $S = 289\pi \text{ nm}^2$, respectively. The aspect ratio of the ellipse is assumed to be $R_{\text{asp}} = 3$. We also performed simulations for circular MTJ, $R_{\text{asp}} = 1$, for comparison.

The initial state of the simulation is prepared by relaxing the magnetization at $T = 300 \text{ K}$ with $K_{\text{eff}} = K_{\text{eff}}^{(0)} (> 0)$ for 10 ns from the equilibrium direction at $T = 0 \text{ K}$ with $m_z > 0$ [27]. Then, the magnetization dynamics at $T = 300 \text{ K}$ are calculated under a voltage pulse applied over a duration of t_p (Fig. 1(b)). During the duration of the pulse, K_{eff} is reduced to $K_{\text{eff}}^{(+V)}$ through the VCMA effect (Fig. 1(j)). After the pulse, the anisotropy constant is increased to the initial value of $K_{\text{eff}} = K_{\text{eff}}^{(0)}$, and there the magnetization is relaxed at $T = 300 \text{ K}$ for 10 ns. The success or failure of switching is determined by the sign of m_z after 10 ns of relaxation. The demagnetization coefficient of the FL is $N_x = 0.01817$, $N_y = 0.08445$, $N_z = 0.89738$ [28], and the magnitude of the IDF is $H_D (= 63.3 \text{ kA}/\text{m}) = 795 \text{ Oe}$ [25]. The WERs are calculated from 10^6 trials.

3. Results

3.1. Upper and lower boundaries of $K_{\text{eff}}^{(+V)}$ for dynamic switching

The equilibrium magnetization direction at $T = 0$ and $V = 0$ is obtained by minimizing the energy density at $V = 0$, $\mathcal{E}^{(0)}$. Figure 2(a) shows the contour plot of $\mathcal{E}^{(0)}$ at $H_{\text{ext}} = 800$ Oe on the ϕ - m_z plane, where the equilibrium directions, $\mathbf{m}^{(0)} = (m_x^{(0)}, m_y^{(0)}, m_z^{(0)}) = (0, 0.258, \pm 0.966)$, are indicated by the open circles. The application of a bias voltage reduces the anisotropy constants from $K_{\text{eff}}^{(0)}$ to $K_{\text{eff}}^{(+V)}$ and destabilizes the initial state. Under appropriate conditions of $K_{\text{eff}}^{(0)}$ and $K_{\text{eff}}^{(+V)}$, the precessional motion of magnetization around the effective magnetic field is induced [29]. As shown in Fig. 2(b), at $K_{\text{eff}}^{(+V)} = -60$ kJ/m³, two equilibrium directions indicated by the open circles are connected by the closed thick gray contour. Therefore, using the precession when the pulse yielding $K_{\text{eff}}^{(+V)} = -60$ kJ/m³ is applied for the half period of precession, the direction of the magnetization can be switched from one equilibrium direction to the other.

The analytical expression of the upper and lower boundaries of $K_{\text{eff}}^{(+V)}$ for dynamic switching is obtained by analyzing the stability of the equilibrium direction [29, 21, 22]. For the small applied field satisfying $0 < H_{\text{ext}} < M_s(N_y - N_x)$, the lower boundary is given by

$$K_{\text{eff,L}} = \frac{\mu_0 M_s^2 (N_x - N_y)}{2} - \frac{\mu_0 M_s H_{\text{ext}}}{1 - m_y^{(0)}}, \quad (4)$$

where

$$m_y^{(0)} = \frac{\mu_0 M_s H_{\text{ext}}}{2K_u^{(0)} + \mu_0 M_s^2 (N_y - N_z)}. \quad (5)$$

The upper boundary is given by [22]

$$K_{\text{eff,U}} = \frac{\mu_0}{2 \left[1 - \left(m_y^{(0)} \right)^2 \right] N_{yx}} \left\{ H_{\text{ext}}^2 - 2M_s H_{\text{ext}} m_y^{(0)} N_{yx} + M_s^2 N_{yx} \left[N_z - N_x - \left(m_y^{(0)} \right)^2 (N_z - N_y) \right] \right\} - \frac{1}{2} \mu_0 M_s^2 (N_z - N_x), \quad (6)$$

where $N_{yx} = N_y - N_x$. For the external magnetic field satisfying $M_s(N_y - N_x) \leq H_{\text{ext}} < 2K_u^{(0)}/(\mu_0 M_s) + M_s(N_y - N_z)$, the lower boundary is the same as Eq. (4) while the upper boundary becomes [22]

$$K_{\text{eff,U}} = \frac{\mu_0 M_s H_{\text{ext}}}{m_y^{(0)} + 1} - \frac{\mu_0 M_s^2 (N_y - N_x)}{2}. \quad (7)$$

Increasing the external magnetic field reduces the energy barrier between the two equilibrium directions. When the external magnetic field is larger than $2K_u^{(0)}/(\mu_0 M_s) + M_s(N_y - N_z)$, the energy barrier vanishes and system has one equilibrium direction at $m_y^{(0)} = 1$. The information cannot be stored as the direction of the magnetization under such a strong magnetic field.

3.2. t_p , $K_{\text{eff}}^{(+V)}$, and H_{ext} dependence of WER

Figures 3(a) and 3(b) shows examples of the WER of the circular and elliptical MTJs. The thickness and area of the FL is the same for both circular and elliptical MTJs. The demagnetizing coefficient for the circular MTJ is $N_x = N_y = 0.04447$ and $N_z = 0.91106$ [28]. The other parameters, except for H_{ext} and $K_{\text{eff}}^{(+V)}$, are the same for all calculations. We calculated the WER for wide range of $K_{\text{eff}}^{(+V)}$ and H_{ext} and found that the optimal value of $(H_{\text{ext}}, K_{\text{eff}}^{(+V)})$ is (400 Oe, 0 kJ/m³) for the circular MTJ and (800 Oe, -60 kJ/m³) for the elliptical MTJ.

The WER of the circular MTJ exhibits the minimum value of $(\text{WER})_{\text{min}} = 2.6 \times 10^{-4}$ at $t_p = 0.43$ ns, as shown in Fig. 3(a). The effective field during the precession comprises only the external field, and the optimal value of the pulse duration is approximately the half of the precession period, i.e., $t_{p,\text{opt}}^{(\text{circle,analytical})} = \pi(1 + \alpha^2)/(\gamma_0 H_{\text{ext}}) = 0.45$ ns. Note that, in the circular MTJ with $N_x = N_y$ and the optimal $K_{\text{eff}}^{(+V)} = 0$, the half of the precession period is $t_{p,\text{opt}}^{(\text{circle,analytical})}$ regardless of the initial direction of magnetization which is thermally fluctuated. Therefore, the distribution of the magnetization direction is kept small during the precession, and subsequently WER is minimized [12]. However, in the elliptical MTJ with $N_x \neq N_y$, this method cannot be applied.

The WER of the elliptical MTJ for $K_{\text{eff}}^{(+V)} = 0$ exhibits a minimum value of $(\text{WER})_{\text{min}} = 2.5 \times 10^{-2}$ at $t_p = 0.31$ ns. The WER is lowered by decreasing $K_{\text{eff}}^{(+V)}$. In the case of $K_{\text{eff}}^{(+V)} = -60$ kJ/m³, $(\text{WER})_{\text{min}} = 3.2 \times 10^{-5}$ is obtained at $t_p = 0.20$ ns. This optimal t_p is about the half of the precession

period, and is shorter than $t_{p,\text{opt}}^{(\text{circle,analytical})}$ at $H_{\text{ext}} = 800$ Oe, 0.23 ns. The precession period is shortened by IDF and NOAF. Note that IDF is induced by the elliptical-cylinder shape, and NOAF by the negative $K_{\text{eff}}^{(+V)}$ can be obtained by the increase of bias voltage and/or the VCMA effect. The occurrence of NOAF can be confirmed with the optimal t_p which is shorter than $t_{p,\text{opt}}^{(\text{circle,analytical})}$ at the applied H_{ext} .

The results show that the appropriate combination of the IDF and the voltage-induced NOAF is effective for reducing the WER. The mechanism of the reduction of the switching time by IDF and voltage-induced NOAF is further discussed in Sec. 4.

Figure 4(a) shows the $K_{\text{eff}}^{(+V)}$ dependence of $(\text{WER})_{\text{min}}$ which is the minimum value of WER obtained by minimizing the WER with respect to t_p . The red squares connected with the red lines represent the results for the circular MTJ at $H_{\text{ext}} = 400$ Oe. The blue circles connected with the blue lines represent the results for elliptical MTJ at $H_{\text{ext}} = 800$ Oe. For large positive $K_{\text{eff}}^{(+V)}$, the magnetization does not precess, and the WER is approximately unity. In the limit of large negative $K_{\text{eff}}^{(+V)}$, WER is 0.5. This is because the magnetization precesses around z -axis during the pulse. After the pulse, the magnetization relaxes to the two equilibrium directions with equal probability.

The WER is a convex function of $K_{\text{eff}}^{(+V)}$, and the lower and upper bounds of $K_{\text{eff}}^{(+V)}$ for dynamic switching are given by Eqs. (4), (6), and (7). For circular MTJ at $H_{\text{ext}} = 400$ Oe, $K_{\text{eff,L}}^{(c)} = -46.2$ kJ/m³ and $K_{\text{eff,U}}^{(c)} = 32.5$ kJ/m³. The lower and upper bounds for dynamic switching of the elliptical MTJ are $K_{\text{eff,L}} = -141$ kJ/m³ and $K_{\text{eff,U2}} = 22.7$ kJ/m³, respectively. The region for dynamic switching is spread and shifts to the negative $K_{\text{eff}}^{(+V)}$ by the IDF or ellipticity as shown in Fig. 4(a). As a result, the elliptical MTJ can be used in wider range of $K_{\text{eff}}^{(+V)}$ or V_p than the circular MTJ.

Figure 4(b) shows H_{ext} dependence of $[\text{WER}]_{\text{min}}$ which is the minimum value of $(\text{WER})_{\text{min}}$ in the $K_{\text{eff}}^{(+V)}$ dependence. The red squares connected with red lines represent the results for circular MTJ at $K_{\text{eff}}^{(+V)} = 0$ kJ/m³. The blue circles connected with blue lines represent the results for elliptical MTJ at $K_{\text{eff}}^{(+V)} = -60$ kJ/m³. For both MTJs, the $[\text{WER}]_{\text{min}}$ is a convex function of H_{ext} . The decrease of $[\text{WER}]_{\text{min}}$ with increase of H_{ext} in the small H_{ext} region is due to the decrease of the precession period or the switching time. The increase of the WER with increase of H_{ext} in the large H_{ext} region is

due to the decrease of energy barrier between the two equilibrium directions. In the absence of the external field, the energy barrier between $(m_x, m_y, m_z) = (0, 0, \pm 1)$ and $(0, 1, 0)$ in the elliptical MTJ is higher than that in the circular MTJ because of the in-plane demagnetizing field. The enhanced energy barrier in the elliptical MTJ can endure large in-plane H_{ext} , that is, the initial state is stable even at large H_{ext} in the elliptical MTJ [22]. Therefore, the optimal value of H_{ext} that minimize $[\text{WER}]_{\text{min}}$ of the elliptical MTJ (800 Oe) is larger than that of the circular MTJ (400 Oe).

In the [Appendix A](#), α and H_{ext} dependencies of $[\text{WER}]_{\text{min}}$ are shown. In the elliptical MTJ, the optimal value of H_{ext} at $\alpha = 0.075$ and 0.05 are slightly smaller than that at $\alpha = 0.1$, but it is larger than that in the circular MTJs.

4. Discussions

As shown in Figs. 3(a) and (b), the optimal pulse duration of the elliptical MTJ with $K_{\text{eff}}^{(+V)} = -60 \text{ kJ/m}^3$ (0.20 ns) is considerably shorter than the elliptical MTJ with $K_{\text{eff}}^{(+V)} = 0 \text{ kJ/m}^3$ (0.31 ns) and the circular MTJ (0.43 ns). The short switching time has the merit of suppressing errors due to the thermal agitation field during the pulse. To understand the mechanism of the reduction of the switching time by IDF and voltage-induced NOAF, we plot the time evolution of the magnetization at $T = 0 \text{ K}$ and torque of the elliptical MTJ in Figs. 5(a) and 5(b).

The top panel of Fig. 5(a) shows the time evolution of m_x (black), m_y (red), and m_z (blue) of the elliptical MTJ under the pulse yielding $K_{\text{eff}}^{(+V)} = 0 \text{ kJ/m}^3$. The origin of the horizontal axis is set to the beginning of the pulse. Starting from the equilibrium direction with $m_z > 0$, the magnetization precesses around the external field H_{ext} and reaches the direction with $m_x = 0$ at 0.38 ns. Due to the damping and the IDF the trajectory is not a semicircle but a semispiral, where m_y monotonically increases with time.

In the bottom panel Fig. 5(a), we plot the time evolution of the θ component of the torque due to the applied field, Q_H (black), the IDF, Q_D (red), and the effective out-of-plane anisotropy field, Q_K (blue). The torques are defined by the equation of motion of θ as

$$\frac{d\theta}{d\tau} = Q_H + Q_D + Q_K, \quad (8)$$

where

$$Q_H = \frac{H_{\text{ext}}}{M_s} (\cos \phi + \alpha \cos \theta \sin \phi), \quad (9)$$

$$Q_D = (N_x - N_y) \sin \theta \sin \phi (\cos \phi + \alpha \cos \theta \sin \phi), \quad (10)$$

$$Q_K = -\frac{\alpha K_{\text{eff}}^{(+V)} \sin 2\theta}{\mu_0 M_s^2}, \quad (11)$$

and τ is the dimensionless time defined as

$$\tau = \frac{\gamma_0 M_s}{1 + \alpha^2} t. \quad (12)$$

As shown in the bottom panel Fig. 5(a), Q_H accelerates the switching dynamics, while Q_D decelerates the switching dynamics. Q_K is zero because $K_{\text{eff}}^{(+V)} = 0$ kJ/m³. Note that the deceleration of the switching dynamics by the negative Q_D increases switching time and therefore WER.

The switching dynamics considerably changes when $K_{\text{eff}}^{(+V)}$ is reduced down to -60 kJ/m³ as shown in the top panel of Fig. 5(b). The y -component of the magnetization, m_y , oscillates and becomes negative around 0.1 ns. The switching time is as small as 0.20 ns, which is almost half of that for $K_{\text{eff}}^{(+V)} = 0$ kJ/m³. The reduction of the switching time is caused by the positive Q_D around 0.1 ns. The results shown in Fig. 5(b) demonstrate that the NOAF induces the rotation of \mathbf{m} around z -axis, making m_y negative. Then, the in-plane anisotropy field, that is IDF, rotates \mathbf{m} around the x -axis, thereby accelerating the switching dynamics and reducing WER in the elliptical MTJ. Note that, in the circular MTJ, $Q_D (= 0)$ shown in Eq. 10 cannot accelerate the switching dynamics because $N_x = N_y$.

Figure 6(a) shows the distribution of energy difference between the magnetization directions at the end of the pulse and the equilibrium direction in the unit of $k_B T$. The parameters are set to the optimal values, $K_{\text{eff}}^{(+V)} = -60$ kJ/m³, $H_{\text{ext}} = 800$ Oe, and $t_p = 0.20$ ns. The shift of the peak of the distribution from zero is caused by Gilbert damping. The mean and standard deviation are $5.6 k_B T$ and $3.4 k_B T$, respectively. Figure 6(b) shows the $K_{\text{eff}}^{(+V)}$ dependence of the mean (red circles) and standard deviation (blue squares) of the energy difference between the magnetization directions at the end of

the pulse and the equilibrium direction. The external in-plane magnetic field is set as $H_{\text{ext}} = 800$ Oe. At each $K_{\text{eff}}^{(+V)}$, t_p is set to the optimal values that minimize the WER there. The mean of the energy difference is minimized around $K_{\text{eff}}^{(+V)} = -60$ kJ/m³ which is the optimal value at which the WER is minimized. The standard deviation of the energy difference is minimized at $K_{\text{eff}}^{(+V)} = -80$ kJ/m³.

The standard deviation is a measure of how large the distribution is spread during the pulse and should decrease with decrease of the switching time. Moreover, the mean is a measure of how close the magnetization at the end of the pulse is to the equilibrium direction. The mean depends not only on the switching time but also on the details of torques during the pulse. Therefore, the value of $K_{\text{eff}}^{(+V)}$ that minimizes the mean should not be the same as that minimizes the standard deviation. However, the results show that both mean and standard deviation are minimized at $K_{\text{eff}}^{(+V)}$ close to the optimal value. The appropriate combination of the IDF and voltage-induced NOAF reduces not only the switching time but also the energy difference between the magnetization directions at the end of the pulse and the equilibrium direction. As a result, the WER is minimized at the optimal value of t_p , H_{ext} , and $K_{\text{eff}}^{(+V)}$.

5. Conclusions

We theoretically analyzed the WER of voltage-induced switching for the VC-MRAM and showed that the appropriate combination of the in-plane demagnetizing field and voltage-induced negative out-of-plane anisotropy field reduces the WER by one order of magnitude compared with that of the dynamic switching in a conventional MTJ. The mechanism of WER reduction is discussed based on the magnetization dynamics at $T = 0$ K and the distribution of the energy difference between the magnetization directions at the end of the pulse and the equilibrium direction at $T = 300$ K. Furthermore, we show that the reduction of the switching time and the mean of the energy difference by the in-plane demagnetizing field and voltage-induced negative out-of-plane anisotropy field causes the reduction of WER. The results provide a guide for designing a reliable VC-MRAM.

6. Acknowledgements

This study is partly based on results obtained from a project, JPNP16007, commissioned by the New Energy and Industrial Technology Development Organization (NEDO), Japan.

Appendix A. H_{ext} dependence of the WER

Figure A.7 shows α and H_{ext} dependencies of $[\text{WER}]_{\text{min}}$. For both the circular MTJ and the elliptical MTJ, $[\text{WER}]_{\text{min}}$ decreases with decrease of α because the magnitude of the thermal agitation field is proportional to $\sqrt{\alpha}$.

In the circular MTJ with $\alpha = 0.1, 0.075$ and 0.05 , the minimum $[\text{WER}]_{\text{min}}$ is yielded by the optimal conditions, $K_{\text{eff}}^{(+V)} = 0 \text{ kJ/m}^3$ and $H_{\text{ext}} = 400 \text{ Oe}$. In the elliptical MTJ with $\alpha = 0.1, (0.075 \text{ and } 0.05)$, the minimum $[\text{WER}]_{\text{min}}$ is yielded by the optimal conditions, $K_{\text{eff}}^{(+V)} = -60 \text{ kJ/m}^3, (-60 \text{ kJ/m}^3 \text{ and } -60 \text{ kJ/m}^3)$, and $H_{\text{ext}} = 800 \text{ Oe}, (700 \text{ Oe and } 700 \text{ Oe})$, respectively. The elliptical MTJ with smaller α does not require $H_{\text{ext}} = 800 \text{ Oe}$ where the reduction of energy barrier and the stability of the initial states are more serious than the reduction of the switching time.

References

- [1] M. Weisheit, S. Fähler, A. Marty, Y. Souche, C. Poinsignon, D. Givord, Electric field-induced modification of magnetism in thin-film ferromagnets, *Science* 315 (5810) (2007) 349–351. [doi:10.1126/science.1136629](https://doi.org/10.1126/science.1136629).
URL <http://science.sciencemag.org/content/315/5810/349>
- [2] T. Maruyama, Y. Shiota, T. Nozaki, K. Ohta, N. Toda, M. Mizuguchi, A. A. Tulapurkar, T. Shinjo, M. Shiraishi, S. Mizukami, Y. Ando, Y. Suzuki, Large voltage-induced magnetic anisotropy change in a few atomic layers of iron, *Nat. Nano.* 4 (3) (2009) 158–161. [doi:10.1038/nnano.2008.406](https://doi.org/10.1038/nnano.2008.406).
URL <http://www.nature.com/nnano/journal/v4/n3/full/nnano.2008.406.html>
- [3] C.-G. Duan, J. P. Velev, R. F. Sabirianov, Z. Zhu, J. Chu, S. S. Jaswal, E. Y. Tsymlal, Surface magnetoelectric effect in ferromagnetic metal films, *Phys. Rev. Lett.* 101 (13) (2008) 137201.

[doi:10.1103/PhysRevLett.101.137201](https://doi.org/10.1103/PhysRevLett.101.137201).

URL <http://link.aps.org/doi/10.1103/PhysRevLett.101.137201>

- [4] K. Nakamura, R. Shimabukuro, Y. Fujiwara, T. Akiyama, T. Ito, A. J. Freeman, Giant modification of the magnetocrystalline anisotropy in transition-metal monolayers by an external electric field, *Phys. Rev. Lett.* 102 (18) (2009) 187201. [doi:10.1103/PhysRevLett.102.187201](https://doi.org/10.1103/PhysRevLett.102.187201).
URL <http://link.aps.org/doi/10.1103/PhysRevLett.102.187201>
- [5] M. Tsujikawa, T. Oda, Finite electric field effects in the large perpendicular magnetic anisotropy surface Pt/Fe/Pt(001): A first-principles study, *Phys. Rev. Lett.* 102 (24) (2009) 247203. [doi:10.1103/PhysRevLett.102.247203](https://doi.org/10.1103/PhysRevLett.102.247203).
URL <http://link.aps.org/doi/10.1103/PhysRevLett.102.247203>
- [6] M. Endo, S. Kanai, S. Ikeda, F. Matsukura, H. Ohno, Electric-field effects on thickness dependent magnetic anisotropy of sputtered MgO/Co₄₀Fe₄₀B₂₀/Ta structures, *Appl. Phys. Lett.* 96 (21) (2010) 212503. [doi:10.1063/1.3429592](https://doi.org/10.1063/1.3429592).
URL <http://aip.scitation.org/doi/10.1063/1.3429592>
- [7] Y. Shiota, T. Nozaki, F. Bonell, S. Murakami, T. Shinjo, Y. Suzuki, Induction of coherent magnetization switching in a few atomic layers of FeCo using voltage pulses, *Nat. Mater.* 11 (1) (2012) 39–43. [doi:10.1038/nmat3172](https://doi.org/10.1038/nmat3172).
URL <http://www.nature.com/nmat/journal/v11/n1/full/nmat3172.html>
- [8] Y. Shiota, S. Miwa, T. Nozaki, F. Bonell, N. Mizuochi, T. Shinjo, H. Kubota, S. Yuasa, Y. Suzuki, Pulse voltage-induced dynamic magnetization switching in magnetic tunneling junctions with high resistance-area product, *Appl. Phys. Lett.* 101 (10) (2012) 102406. [doi:10.1063/1.4751035](https://doi.org/10.1063/1.4751035).
URL <http://aip.scitation.org/doi/10.1063/1.4751035>
- [9] S. Kanai, M. Yamanouchi, S. Ikeda, Y. Nakatani, F. Matsukura, H. Ohno, Electric field-induced magnetization reversal in a perpendicular-anisotropy CoFeB-MgO magnetic tunnel junction, *Appl. Phys. Lett.* 101 (12) (2012) 122403. [doi:10.1063/1.4753816](https://doi.org/10.1063/1.4753816).
URL <http://aip.scitation.org/doi/10.1063/1.4753816>

- [10] Y. Shiota, T. Nozaki, S. Tamaru, K. Yakushiji, H. Kubota, A. Fukushima, S. Yuasa, Y. Suzuki, Evaluation of write error rate for voltage-driven dynamic magnetization switching in magnetic tunnel junctions with perpendicular magnetization, *Appl. Phys. Express* 9 (1) (2016) 013001. doi:10.7567/APEX.9.013001.
URL <http://iopscience.iop.org/article/10.7567/APEX.9.013001/meta>
- [11] C. Grezes, F. Ebrahimi, J. G. Alzate, X. Cai, J. A. Katine, J. Langer, B. Ocker, P. Khalili Amiri, K. L. Wang, Ultra-low switching energy and scaling in electric-field-controlled nanoscale magnetic tunnel junctions with high resistance-area product, *Appl. Phys. Lett.* 108 (1) (2016) 012403. doi:10.1063/1.4939446.
URL <http://aip.scitation.org/doi/abs/10.1063/1.4939446>
- [12] Y. Shiota, T. Nozaki, S. Tamaru, K. Yakushiji, H. Kubota, A. Fukushima, S. Yuasa, Y. Suzuki, Reduction in write error rate of voltage-driven dynamic magnetization switching by improving thermal stability factor, *Appl. Phys. Lett.* 111 (2) (2017) 022408. doi:10.1063/1.4990680.
URL <http://aip.scitation.org/doi/10.1063/1.4990680>
- [13] T. Yamamoto, T. Nozaki, Y. Shiota, H. Imamura, S. Tamaru, K. Yakushiji, H. Kubota, A. Fukushima, Y. Suzuki, S. Yuasa, Thermally induced precession-orbit transition of magnetization in voltage-driven magnetization switching, *Phys. Rev. Applied* 10 (2) (2018) 024004. doi:10.1103/PhysRevApplied.10.024004.
URL <https://link.aps.org/doi/10.1103/PhysRevApplied.10.024004>
- [14] T. Yamamoto, T. Nozaki, H. Imamura, Y. Shiota, S. Tamaru, K. Yakushiji, H. Kubota, A. Fukushima, Y. Suzuki, S. Yuasa, Improvement of write error rate in voltage-driven magnetization switching, *J. Phys. D: Appl. Phys.* 52 (16) (2019) 164001. doi:10.1088/1361-6463/ab03c2.
URL <https://doi.org/10.1088/1361-6463/ab03c2>
- [15] S. Yuasa, T. Nagahama, A. Fukushima, Y. Suzuki, K. Ando, Giant room-temperature magnetoresistance in single-crystal Fe/MgO/Fe

- magnetic tunnel junctions, *Nat. Mater.* 3 (12) (2004) 868–871.
[doi:10.1038/nmat1257](https://doi.org/10.1038/nmat1257).
URL <http://www.nature.com/nmat/journal/v3/n12/full/nmat1257.html>
- [16] S. S. P. Parkin, C. Kaiser, A. Panchula, P. M. Rice, B. Hughes, M. Samant, S.-H. Yang, Giant tunnelling magnetoresistance at room temperature with MgO (100) tunnel barriers, *Nat. Mater.* 3 (12) (2004) 862–867. [doi:10.1038/nmat1256](https://doi.org/10.1038/nmat1256).
URL <http://www.nature.com/nmat/journal/v3/n12/full/nmat1256.html>
- [17] D. D. Djayaprawira, K. Tsunekawa, M. Nagai, H. Maehara, S. Yamagata, N. Watanabe, S. Yuasa, Y. Suzuki, K. Ando, 230% room-temperature magnetoresistance in CoFeB/MgO/CoFeB magnetic tunnel junctions, *Appl. Phys. Lett.* 86 (9) (2005) 092502. [doi:10.1063/1.1871344](https://doi.org/10.1063/1.1871344).
URL <http://scitation.aip.org/content/aip/journal/apl/86/9/10.1063/1.1871344>
- [18] C. Davies, K. Prabhakara, M. D. Davydova, K. A. Zvezdin, T. B. Shapava, S. Wang, A. K. Zvezdin, A. Kirilyuk, T. Rasing, A. V. Kimel, Anomalous damped heat-assisted route for precessional magnetization reversal in an iron garnet, *Phys. Rev. Lett.* 122 (2) (2019) 027202. [doi:10.1103/PhysRevLett.122.027202](https://doi.org/10.1103/PhysRevLett.122.027202).
URL <https://link.aps.org/doi/10.1103/PhysRevLett.122.027202>
- [19] S. Kanai, F. Matsukura, H. Ohno, Electric-field-induced magnetization switching in CoFeB/MgO magnetic tunnel junctions with high junction resistance, *Appl. Phys. Lett.* 108 (19) (2016) 192406. [doi:10.1063/1.4948763](https://doi.org/10.1063/1.4948763).
URL <https://aip.scitation.org/doi/10.1063/1.4948763>
- [20] D. Apalkov, B. Dieny, J. M. Slaughter, Magnetoresistive random access memory, *Proceedings of the IEEE* 104 (10) (2016) 1796–1830. [doi:10.1109/JPROC.2016.2590142](https://doi.org/10.1109/JPROC.2016.2590142).
- [21] R. Matsumoto, T. Sato, H. Imamura, Voltage-induced switching with long tolerance of voltage-pulse duration in a perpendicularly

- magnetized free layer, *Appl. Phys. Express* 12 (5) (2019) 053003.
[doi:10.7567/1882-0786/ab1349](https://doi.org/10.7567/1882-0786/ab1349).
URL <https://doi.org/10.7567/1882-0786/ab1349>
- [22] R. Matsumoto, S. Yuasa, H. Imamura, Heavily damped precessional switching with very low write-error rate in elliptical-cylinder magnetic tunnel junctions, *Phys. Rev. Applied* 18 (5) (2022) 054069.
[doi:10.1103/PhysRevApplied.18.054069](https://doi.org/10.1103/PhysRevApplied.18.054069).
URL <https://link.aps.org/doi/10.1103/PhysRevApplied.18.054069>
- [23] Y. J. Yeoh, H. Tamukoh, O. Nomura, H. Arai, H. Imamura, T. Morie, Development of quantization YOLO model and WER tolerance evaluation for VC-MRAM implementation, The 69th JSAP Spring Meeting 2022, The Japan Society of Applied Physics (JSAP), Aoyama Gakuin University Sagamihara Campus, Kanagawa 22a-E102-4.
- [24] M. D. Stiles, J. Miltat, Spin-transfer torque and dynamics, in: *Spin Dynamics in Confined Magnetic Structures III*, edited by Burkard Hillebrands and André Thiaville, in: *Topics in Applied Physics*, vol. 101, Springer Berlin Heidelberg, 2006, pp. 225–308.
[doi:10.1007/10938171_7](https://doi.org/10.1007/10938171_7).
URL https://doi.org/10.1007/10938171_7
- [25] R. Matsumoto, H. Imamura, Critical current density of a spin-torque oscillator with an in-plane magnetized free layer and an out-of-plane magnetized polarizer, *AIP Advances* 6 (12) (2016) 125033.
[doi:10.1063/1.4972263](https://doi.org/10.1063/1.4972263).
URL <https://aip.scitation.org/doi/10.1063/1.4972263>
- [26] W. F. Brown, Jr., Thermal fluctuations of a single-domain particle, *Phys. Rev.* 130 (5) (1963) 1677–1686.
[doi:10.1103/PhysRev.130.1677](https://doi.org/10.1103/PhysRev.130.1677).
URL <http://link.aps.org/doi/10.1103/PhysRev.130.1677>
- [27] H. Imamura, H. Arai, R. Matsumoto, Distribution of write error rate of spin-transfer-torque magnetoresistive random access memory caused by a distribution of junction parameters, *Journal of Magnetism and Magnetic Materials* 563 (2022) 170012.
[doi:https://doi.org/10.1016/j.jmmm.2022.170012](https://doi.org/10.1016/j.jmmm.2022.170012).

URL <https://www.sciencedirect.com/science/article/pii/S0304885322008976>

- [28] M. Beleggia, M. D. Graef, Y. T. Millev, D. A. Goode, G. Rowlands, Demagnetization factors for elliptic cylinders, *J. Phys. D: Appl. Phys.* 38 (18) (2005) 3333. doi:10.1088/0022-3727/38/18/001.

URL <https://dx.doi.org/10.1088/0022-3727/38/18/001>

- [29] R. Matsumoto, T. Nozaki, S. Yuasa, H. Imamura, Voltage-induced precessional switching at zero-bias magnetic field in a conically magnetized free layer, *Phys. Rev. Applied* 9 (1) (2018) 014026. doi:10.1103/PhysRevApplied.9.014026.

URL <https://link.aps.org/doi/10.1103/PhysRevApplied.9.014026>

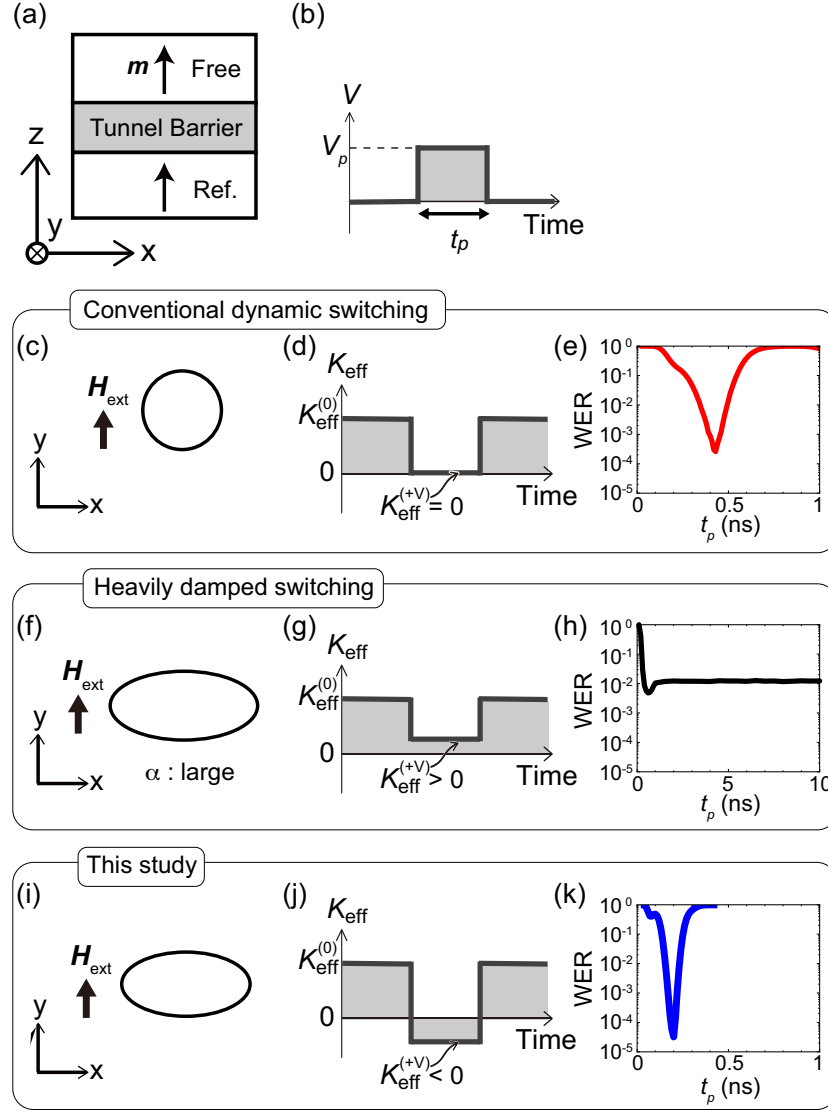


Figure 1: (a) Cross-section of a magnetic tunnel junction (MTJ) with a perpendicularly-magnetized free layer and a reference (Ref.) layer, and the Cartesian coordinates defined as (x, y, z) . (b) Shape of the voltage pulse. The amplitude and duration of the pulse are V_p (positive value) and t_p , respectively. (c) Top view of the MTJ and the direction of the external magnetic field, \mathbf{H}_{ext} , used in the conventional precessional switching (CPS) scheme. A small Gilbert damping constant, α , is preferred. (d) Temporal variation of the effective out-of-plane anisotropy constant, K_{eff} , used in the CPS scheme. (e) An example of t_p dependence of the write error rate (WER) obtained by the CPS scheme. (f) Top view of the MTJ and the direction of \mathbf{H}_{ext} used in the heavily damped switching (HDS) scheme. A large α is preferred. (g) Temporal variation of K_{eff} used in the HDS scheme. (h) Typical example of t_p dependence of WER obtained by the HDS scheme. (i) Top view of the MTJ and the direction of \mathbf{H}_{ext} used in the switching scheme proposed in this study. A small α is preferred. (j) Temporal variation of K_{eff} used in this study. (k) Typical example of t_p dependence of WER obtained in this study. In (d), (g), (j), $K_{\text{eff}}^{(0)}$ and $K_{\text{eff}}^{(+V)}$ denote K_{eff} at voltage amplitudes of $V = 0$ and $V = V_p$, respectively.

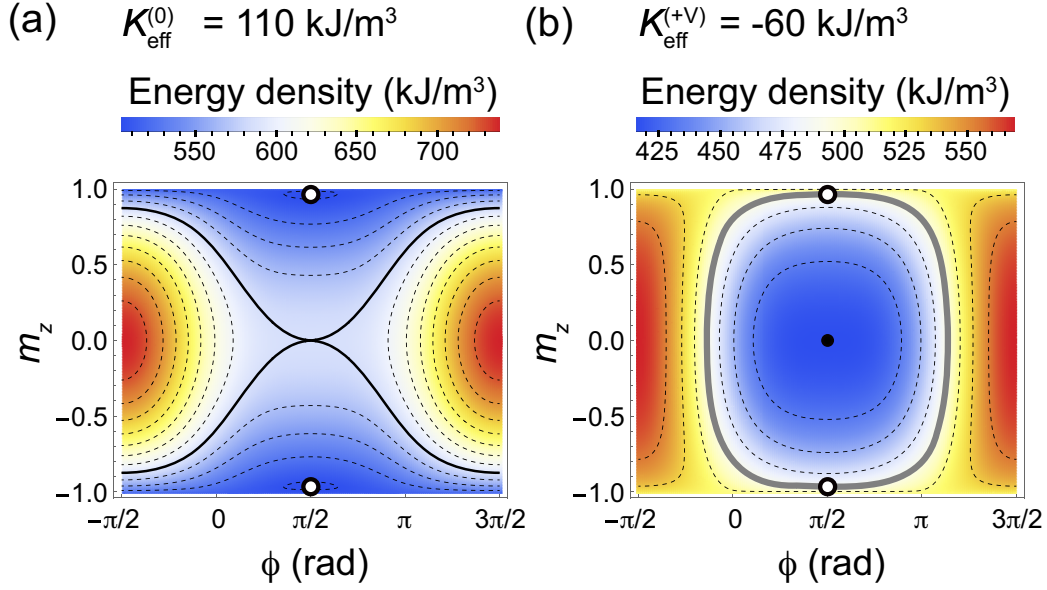


Figure 2: (a) Contour plot of the energy density at $V = 0$ on the ϕ - m_z plane. The effective out-of-plane anisotropy constant is $K_{\text{eff}}^{(0)} = 110 \text{ kJ/m}^3$. The solid black curve represents the energy contour crossing the saddle point at $(\phi, m_z) = (\pi/2, 0)$, i.e., the separatrix. The open circles indicate the equilibrium directions, $\mathbf{m}^{(0)}$. (b) Contour plot of the energy density during the pulse with $K_{\text{eff}}^{(+V)} = -60 \text{ kJ/m}^3$. The open circles indicate the equilibrium directions, $\mathbf{m}^{(0)}$. The thick gray contour represents the contour with the same energy density as $\mathcal{E}(\mathbf{m}^{(0)})$, corresponding to the trajectory of the magnetization precession with $\alpha = 0$ at $T = 0 \text{ K}$.

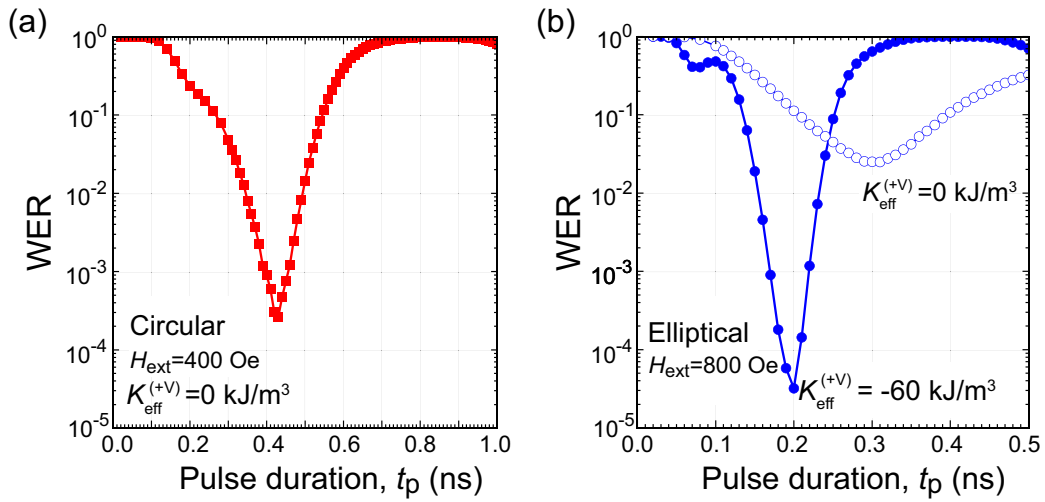


Figure 3: (a) Pulse duration, t_p , dependence of WER for circular MTJ under $H_{\text{ext}} = 400$ Oe. The effective out-of-plane anisotropy constant during the pulse is $K_{\text{eff}}^{(+V)} = 0$ kJ/m³. The minimum value of the WER, $(\text{WER})_{\text{min}}$, is 2.6×10^{-4} . (b) Pulse duration dependence of WER for elliptical MTJ under $H_{\text{ext}} = 800$ Oe. The results for $K_{\text{eff}}^{(+V)} = 0$ and -60 kJ/m³ are represented by the open and solid circles, respectively. The minimum value of the WER for $K_{\text{eff}}^{(+V)} = 0$ and -60 kJ/m³ are $(\text{WER})_{\text{min}} = 2.5 \times 10^{-2}$ and 3.2×10^{-5} , respectively.

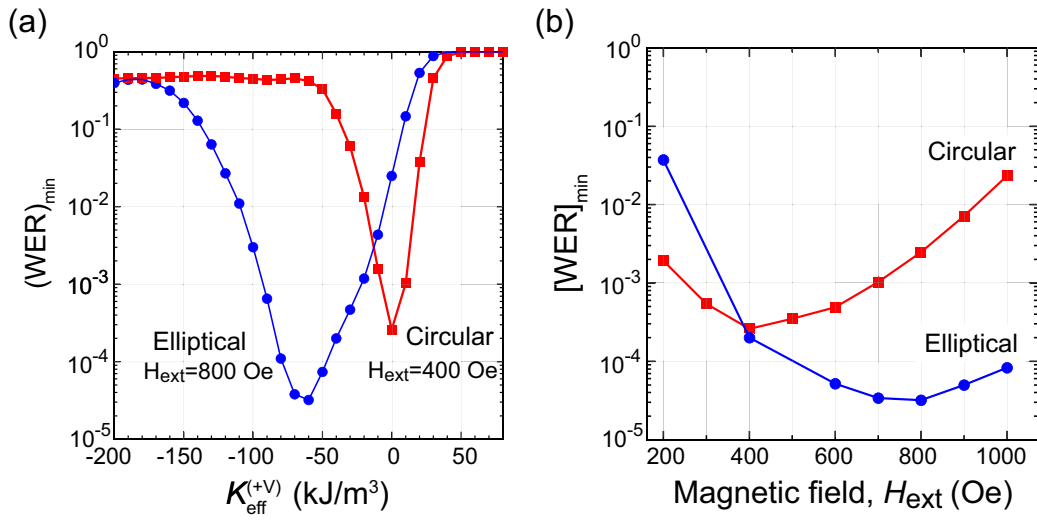


Figure 4: (a) $K_{\text{eff}}^{(+V)}$ dependence of $(\text{WER})_{\min}$, which is the minimum value of WER in the t_p dependence. The results for the circular MTJ at $H_{\text{ext}} = 400$ Oe are represented by red squares connected with red lines. The results for the elliptical MTJ at $H_{\text{ext}} = 800$ Oe are represented by blue circles connected with blue lines. (b) H_{ext} dependence of $[\text{WER}]_{\min}$ which is the minimum value of $(\text{WER})_{\min}$ in the $K_{\text{eff}}^{(+V)}$ dependence. The results for the circular MTJ are represented by red squares connected with red lines. The results for the elliptical MTJ are represented by blue circles connected with blue lines.

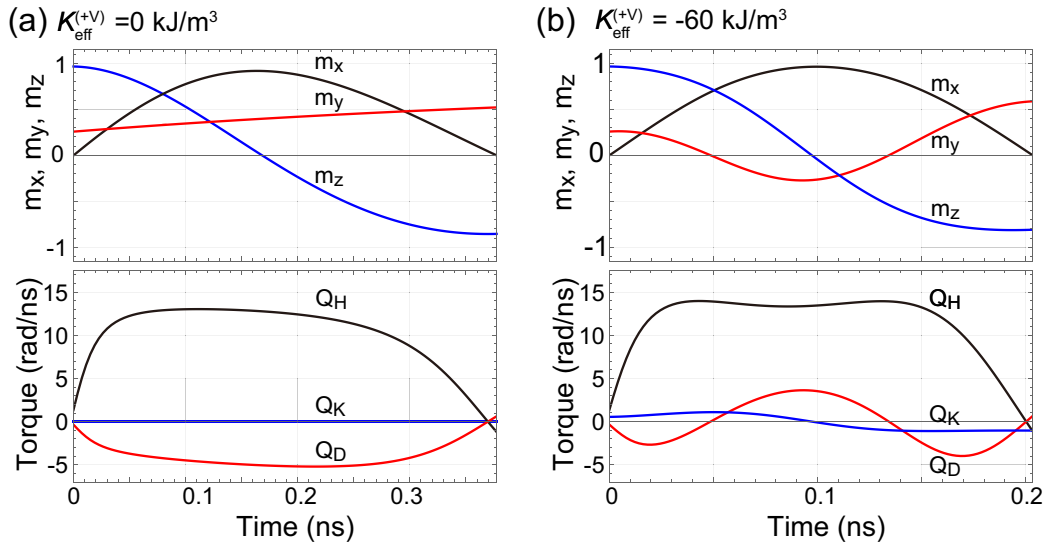


Figure 5: Time evolution of the magnetization and torque of the elliptical MTJ during the pulse at $T = 0 \text{ K}$. (a) Results for the pulse yielding $K_{\text{eff}}^{(+V)} = 0 \text{ kJ/m}^3$. The top panel shows the time evolution of m_x (black), m_y (red), and m_z (blue). The bottom panel show the time evolution of the θ component of the torque due to the external field, Q_H (black), the IDF, Q_D (red), and the effective out-of-plane anisotropy field, Q_K (blue). (b) Same plot for the pulse yielding $K_{\text{eff}}^{(+V)} = -60 \text{ kJ/m}^3$.

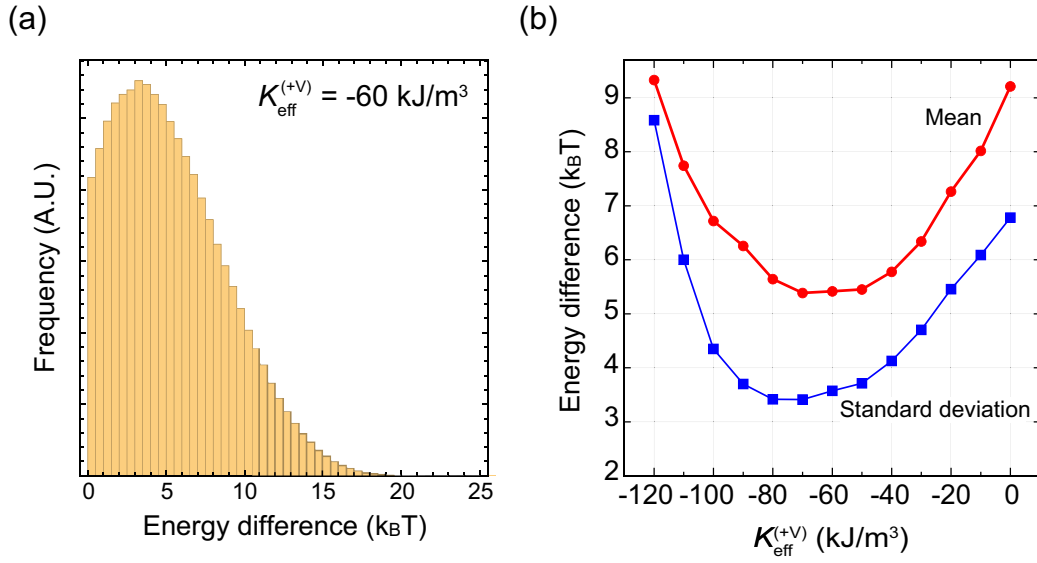


Figure 6: (a) Distribution of the energy difference between the magnetization directions at the end of the pulse and the equilibrium direction in the unit of $k_B T$. The parameters are assumed to be the optimal values, $K_{\text{eff}}^{(+V)} = -60 \text{ kJ/m}^3$, $H_{\text{ext}} = 800 \text{ Oe}$, and $t_p = 0.20 \text{ ns}$. (b) Mean (red circles) and standard deviation (blue squares) of the energy difference between the magnetization directions at the end of the pulse and the equilibrium direction as a function of $K_{\text{eff}}^{(+V)}$. The external in-plane magnetic field is set as $H_{\text{ext}} = 800 \text{ Oe}$. At each $K_{\text{eff}}^{(+V)}$, t_p is set to the optimal values that minimize the WER there.

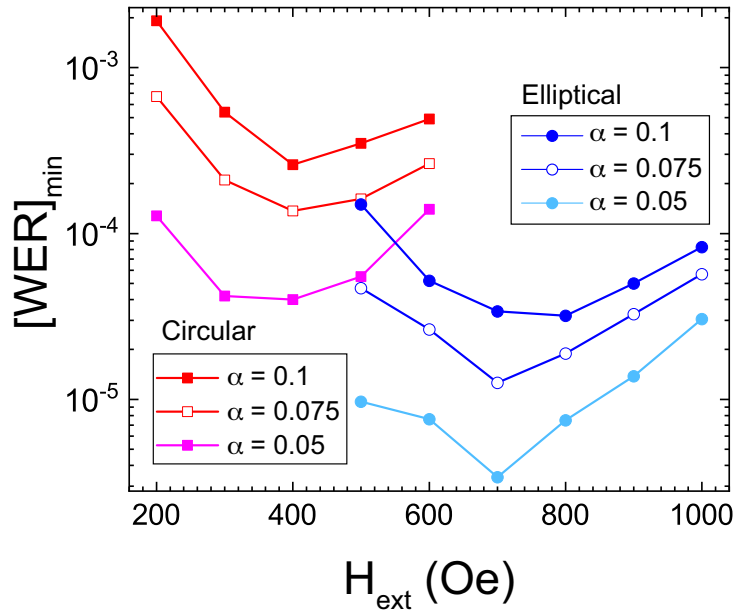


Figure A.7: α and H_{ext} dependencies of $[WER]_{\min}$. The results for the circular MTJ are represented by squares. The results for the elliptical MTJ are represented by the circles. The results for the $\alpha = 0.1$ are the same as those in Fig. 4(b).